Direct and Sensitive Detection of Mercury in Soil by Portable Electromagnetic Heating Vaporization and Purge-and-trap Followed by Microplasma Optical Emission Spectrometry

Zhengqin Pang, [a] Tian Ren, [a] Yuanyuan Liu, [a] Jiahui Yang, [b] Yurong Deng, [a,*] and Chengbin Zheng [a,*]

[a]Key Laboratory of Green Chemistry & Technology of MOE, College of Chemistry, Sichuan University, Chengdu 610064, P. R. China

[b] Analytical & Testing Center, Sichuan University, Chengdu, Sichuan 610064, P. R. China

Received: *April 18, 2024;* ***Revised:*** *May 11, 2024;* ***Accepted:*** *May 11, 2024;* ***Available online:*** *June 09, 2024.*

DOI: 10.46770/AS.2024.115

ABSTRACT: To enhance sample throughput and avoid environmental pollution, it is crucial to develop an atomic spectrometry method for the direct and sensitive detection of heavy metals in soil samples. In this work, a portable analytical device integrating electromagnetic heating evaporation (EMHV), purge-and-trap (P&T), and miniature point discharge optical emission spectrometry (μPD-OES) was developed to determine mercury in soil without chemical pretreatment. This method involves converting soil mercury species into cold mercury vapor (Hg^0), which is then evaporated from the sample using a low-power miniaturized EMHV device. The generated Hg^0 is subsequently separated and trapped in a tube filled with gold-sand before μPD-OES analysis. This process not only preconcentrates the analyte but also achieves complete matrix separation before analysis, thereby reducing matrix interference and enhancing the sensitivity of the mercury detection. Under optimal experimental conditions, the limit of determination (LOD) for mercury was established at 0.25 μg kg^{-1} with a relative standard deviation (RSD) of 3.6% and a sample consumption of 60 mg. The accuracy and practicality of the EMHV-P&T-μPD-OES method were validated through the determination of mercury in two soil certified reference materials (CRMs) and five real soil samples. The analytical results agree well with the certified values of the CRMs, confirming the practicality of the proposed analytical system for soil mercury analysis.

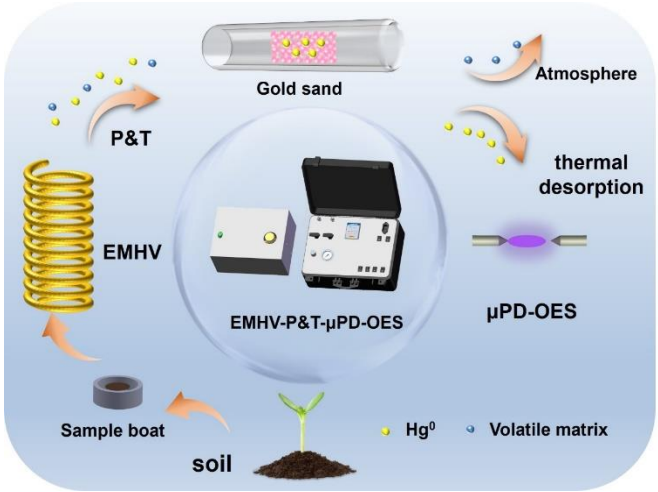

INTRODUCTION

Heavy metal contamination of soil is a global concern due to the non-biodegradability, high toxicity, and bioaccumulation of heavy metals.[1-3] This issue also attracts significant attention regarding public health and agricultural safety, as individuals inevitably consume heavy metals through foods like rice, vegetables, and others grown in contaminated soils.[4-6] Among various heavy metal pollutants, mercury is particularly concerning because of its high toxicity and strong tendency to react with proteins and other biomolecules, especially those containing sulfur and oxygen functional groups.[7] These reactions can lead to toxicological and carcinogenic effects on various organs, including the nervous system,[8] kidneys,[9] and liver.[10] Consequently, substantial efforts have been devoted to developing methods for detecting mercury in soil.[11-13] Techniques such as laser-induced breakdown spectroscopy (LIBS)[14, 15] and X-ray Fluorescence Spectrometry (XRF)[16, 17] are popular due to their cost-effectiveness, minimal sample preparation, and rapid on-site detection capabilities.

However, these methods often suffer from low sensitivity, serious matrix interference, and a lack of solid certified reference materials (CRMs) with matching matrices, rendering them unsuitable for rapid screening of heavy metals in soil samples. Although atomic spectrometric methods offer higher sensitivity, accuracy, and better anti-interference capability capabilities than LIBS and XRF, the commercial instruments required are bulky, expensive, and energy-intensive, which limits their field applicability. Additionally, complete sample digestion is usually necessary before detection using atomic spectrometry to reduce matrix interference and eliminate the need for CRMs with matching matrices.[18, 19] However, conventional sample digestion techniques, such as electrically heated digestion and microwave-assisted digestion, are time-consuming, energy-intensive, and require significant amounts of concentrated mineral acids, making them impractical for field analysis.

Over the past 40 years, various portable atomic spectrometric systems, including tungsten coil electrothermal atomic absorption spectrometry (W-coil ET-AAS),[20] microplasma optical emission spectrometry,[21-24] and W-coil optical emission spectrometry,[25] have been developed for accomplishing elemental field analysis. Optical emission spectrometry, compared to atomic absorption spectrometry, does not require a light source (such as a hollow cathode lamp) and is thus more amenable to miniaturization. Recently, several types of microplasmas have been used to develop compact optical emission spectrometers for field detection of heavy metals. These systems are characterized by their small size, high excitation capability, and low power consumption, including liquid electrode glow discharge (LEGD),[26-29] point discharge (PD) ,[11, 30-32] dielectric barrier discharge (DBD),[22, 33-35] atmospheric pressure glow discharge (APGD),[36-38] and solution cathode glow discharge (SCGD).[39, 40] Despite their proven feasibility for elemental detection and significant performance improvements when coupled with efficient sampling techniques,[11, 30] they have primarily been utilized for environmental water sample analysis due to minimal or no sample pretreatment requirements. A recent development includes a simple, low-power-consuming online digestion unit integrated with a portable PD optical emission spectrometer for detecting Pb in rice and solid biological samples in rice and some solid biological samples[41]. However, the complete digestion of soil samples remains more challenging than that of rice and biological samples. Thus, developing a method for direct field detection of heavy metals in soil with minimal or no chemical pretreatment is highly desirable.

Generally, the direct detection of heavy metals in soil using atomic spectrometry can be readily achieved in the laboratory with techniques such as laser ablation (LA)[42] and electrothermal vaporization (ETV)[43] as sample introduction methods. Compered to LA, ETV is more established for the direct analysis of soil samples due to its effective matrix separation and cost-effective instrumentation. However, the conventional ETV, using graphite,[44] tungsten,[45] molybdenum,[46] rhenium,[47] and other high melting point metals as heating materials, often suffer from low heating efficiencies and high power consumption as sample introduction approaches. To overcome these limitations and adapt ETV suitable for field analytical chemistry, Wang *et al.*[48] and Jiang *et al.*[49] developed an electromagnetic heating vaporization (EMHV) device and employed it in conjunction with microplasma optical emission spectrometry for the direct quantification of Hg, Cd, and Pb in hair and soil samples. Additionally, EMHV offers the advantages of rapid heating and improved reproducibility over conventional ETV. However, both conventional ETV and EMHV sampling techniques are unsuitable for mercury detection using microplasma optical spectrometry, as mercury is a volatile element that tends to vaporize along with volatile organic compounds and moisture, seriously compromising microplasma stability. Moreover, the power consumption of microplasma is typically less than 100 W, with most of the power absorbed by the organic matrices and moisture, resulting in low sensitivity that fails to meet the requirements for detecting ultratrace levels of mercury in liquid or solid samples.

The aim of this work was to introduce a pretreatment method that separates analytes from the vaporized sample matrices before microplasma optical emission spectrometric analysis, thereby improving sensitivity and reducing matrix interference in the detection of heavy metals in soil. To achieve this, a mini purge-and-trap (P&T) unit was integrated into a miniaturized EMHV point discharge optical emission spectrometry (μPD-OES) device. This analytical system not only eliminates the need for chemical pretreatment but also achieves highly efficient matrix separation and preconcentration of analytes prior to analysis, thus simplifying the analytical process, minimizing matrix interference, and significantly enhancing analytical performance. The accuracy and practicality of the device were validated by analyzing two certified reference materials (CRM GSS-3a and GSD-3a) and five real soil samples.

EXPERIMENTAL

Reagents and materials. The boat used to hold the soil sample was custom-made and consisted of an iron crucible (inner diameter: 19 mm, depth: 5 mm, thickness: 1.5 mm) provided by Qinghe Yugan Metal Material Co., Ltd. All solutions in this study were prepared using high-purity deionized water (18.25 MΩ cm) produced by an ultra-pure water machine (PCJ-110, Chengdu Pincheng Technology Co., Ltd., China). High-purity argon (Ar) (≥99.99%) for use in the experimental instrument was sourced from Chengdu Chaohong Gas Company, China. Soil and stream sediment certified reference materials (CRMs) GBW07402a (GSS-2a), GBW07403a (GSS-3a), GBW07405a (GSS-5a),

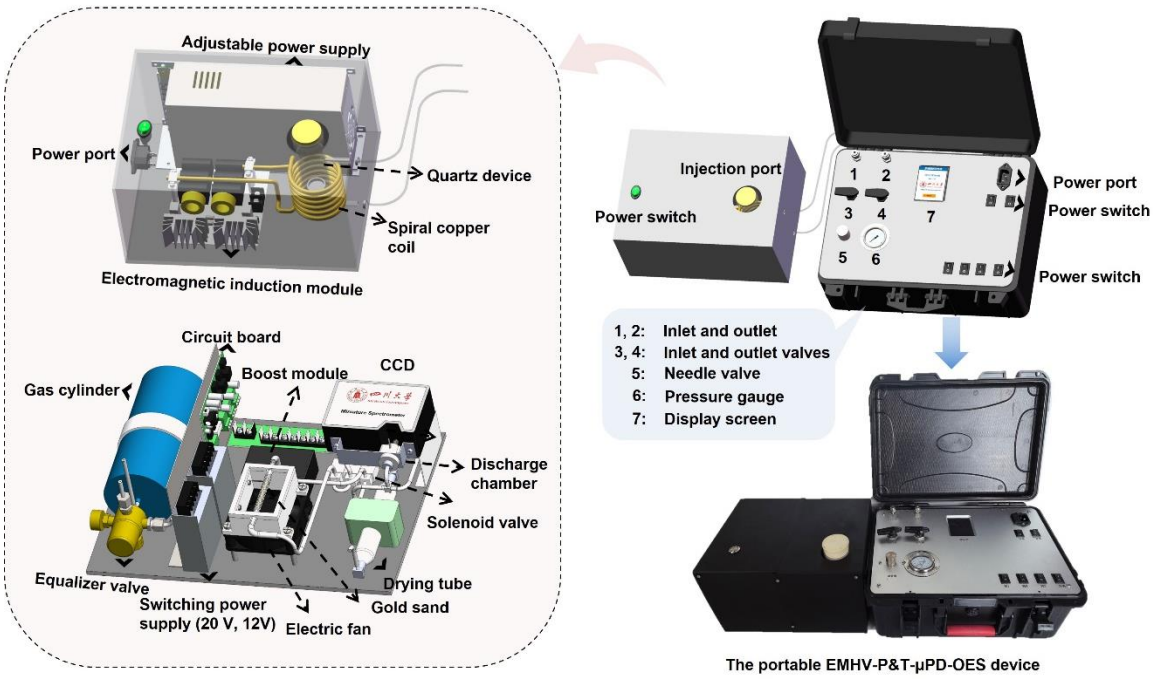

Fig. 1 The portable EMHV-P&T-μPD-OES device.

GBW07980 (GSS-38), and GBW07303a (GSD-3a), along with standard stock solutions of Hg, Fe, As, Mg, Cr, Zn, Pb, Ni, and Cu, were obtained from the National Standard Material Research Centre in Beijing, China. Quartz sand (80-100 mesh, Weihui Kainuo Trading Co., Ltd.) was calcined in a muffle furnace at 850°C for 2 h and subsequently transferred to glass bottles for cooling. Reagents including nitric acid (HNO_3), hydrochloric acid (HCl), potassium borohydride (KBH_4), potassium hydroxide (KOH), and five sodium salts (F^-, SO_4^{2-}, NO_3^-, HPO_4^{2-}, Cl^-) were acquired from Chengdu Colon Chemical Co., Ltd., China. Five soil samples were dried at room temperature for 24 h, with impurities such as branches, hay, and stones removed. These samples were then thoroughly ground, sieved through a 100-mesh screen, and stored in sealed containers at -4°C.

Instrumentation. The analytical device primarily comprised the following components: an electromagnetic heating vaporization unit, a purge-and-trap unit, a miniature point discharge optical emission spectrometry detection unit, the corresponding circuit, and a gas path system. A schematic of the device is depicted in Fig. 1.

The electromagnetic heating vaporization unit operates differently from traditional resistance contact heating devices. It includes an electromagnetic induction module (Shenzhen Zhengpin Source Digital Technology Co., Ltd.), a spiral copper coil, an iron sample boat, and a specially designed evaporation device. The electromagnetic induction module converts the input direct current (DC) into a stable high-frequency alternating current (AC). An alternating magnetic field is generated when the AC passes through a copper coil wrapped around the evaporation device. The sample boat serves both as a carrier for the soil samples and as a medium for heating. The evaporation device itself primarily comprises a 40/38 standard inner grinding port, a large quartz tube (120 mm length × 30 mm i.d. × 34 mm o.d.), a small quartz tube (45 mm length × 20 mm i.d. × 24 mm o.d.), an inlet pipe (10 mm length × 3 mm i.d. × 5 mm o.d.), and an outlet pipe (10 mm length × 3 mm internal diameter × 5 mm outer diameter). A small quartz tube is installed inside the large quartz tube to act as the base for the sample boat.

The main components of the purge-and-trap unit included an adsorption tube filled with gold-sand, a base for stabilization, an electric fan (Dongguan Zhangtou Mu Shentai Electric Co., Ltd., Guangdong, China), and three solenoid valves (Fa0520E, Dongguan Zhirong Vacuum Equipment Co., Ltd., Guangdong, China). The adsorption tube, made of quartz, measured 120 mm in length with an outer diameter of 5 mm and featured varying inner diameters—3 mm for 80 mm of its length and 2 mm for the remaining 40 mm. The gold-sand, occupying a central section approximately 40 mm long, was sealed at both ends with quartz wool to prevent its loss. An electric fan rapidly cooled the adsorption tube after desorption, while the three solenoid valves regulated the flow of carrier and purge gases.

Miniature point discharge optical emission spectrometers, as previously reported,[24, 50-52] include a discharge chamber composed

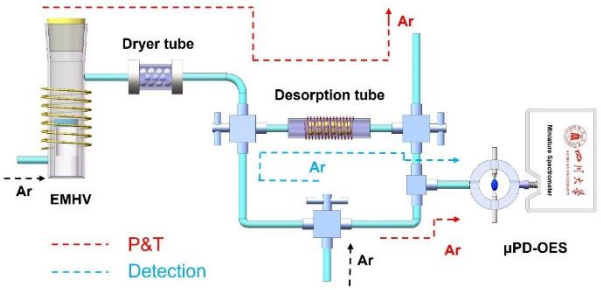

Fig. 2 The schematic diagram of gas circuit of EMHV-P&T-μPD-OES.

of two tapered tungsten electrodes (2 mm) and a PTFE chamber (height 1.5 cm, inner diameter 0.6 cm, outer diameter 2.2 cm). A collimated lens connected to a handheld charge-coupled device (CCD) spectrometer (Maya 2000 Pro, Marine Optical Instruments Corporation, Florida, USA) collected the mercury emission lines.

The entire device's power supply system utilized a high-capacity, compact, portable mobile power supply (H600, Shenzhen Miyang Technology Co., Ltd., Guangdong, China), providing a 220 V AC output port. Three adjustable power supplies converted the 220 V AC voltage to 30 V, 20 V, and 12 V DC input voltages, which powered the electromagnetic induction heating unit, thermal desorption device (Nichrome resistance wire), and circuit board (customized by Medeen Electronic Technology Co., Ltd., Guangdong, China), respectively. The circuit board, equipped with three output ports, allowed for the adjustment of shunt output voltage via a desktop display screen. The power inputs for the cooling fan, three solenoid valves, and the discharge chamber were independently. The gas supply system of the device included a custom-made 0.4 L cylinder housed within the case, an external 4 L Ar gas cylinder, and the corresponding control valve, ensuring a stable flow of high-purity Ar, which functioned as both the discharge carrier gas and the purge gas. The gas connection design is shown in Fig. 2. The EMHV-P&T-μPD-OES device is divided into two processes: "P&T" and "Detection".

Analytical procedure. An appropriate amount of soil CRMs or sample (20-60 mg) was weighed and placed in the sample boat. The electromagnetic heating unit was then connected to the power supply (30 V). The soil was heated for 20 s while a flow rate of Ar (100 mL min^{-1}) was introduced to purge the escaped mercury vapor (Hg^0). Hg^0 was transferred into a gold-sand adsorption tube for pre-concentration. Simultaneously, Ar (80 mL min^{-1}) was introduced directly into the discharge chamber to maintain discharge stability. After 3 min of purging, the purging gas was turned off, and the power supply (12 V) to the three solenoid valves was adjusted to change the direction of the Ar. A thermal desorption power supply (20 V) was then activated to desorb the enriched mercury from the gold-sand. The carrier gas swept the desorbed mercury into the PD discharge chamber for excitation, and the emission of mercury atoms at 253.7 nm was measured using a CCD spectrometer.

Determination of mercury in soil samples by the hydride generation-atomic fluorescence method (HG-AFS). Following the national standard method GB/T 22105.1, the soil samples were initially treated with a nitric acid-hydrochloric acid mixture (HNO_3-HCl) and digested in a boiling water bath. Brief1y, a soil sample (0.2-1 g) was weighed into a 50 mL cuvette. A small amount of deionized water was added to moisten the sample, which was then mixed with 10 mL of [1+1] aqua regia. The cuvette was sealed with a stopper and placed in a boiling water bath for 2 h. After digestion, the sample was cooled to room temperature, diluted with 5% (v/v) nitric acid, shaken thoroughly, and then the supernatant was analyzed using HG-AFS. A blank digestion experiment was also performed. The experimental parameters for the HG-AFS method are as listed in Table S1.

RESULTS AND DISCUSSION

Feasibility of EMHV-P&T-μPD-OES for soil mercury detection. Despite growing interest in mciroplasma optical emission spectrometry over the past decade, its application for the field detection of mercury in soil samples remains limited due to the low power of the microplasma and the complex soil matrix. For instance, volatile organic substances and water contained in the soil are simultaneously vaporized into the microplasma excitation source during EMHV microplasma optical emission spectrometric analysis, significantly impairing the excitation/atomization capacity and stability of the microplasma. This study aimed to eliminate interference from the sample matrix and water vapor during sample analysis. Therefore, a purge-and-trap unit with an adsorption tube filled with gold was employed to separate and preconcentrate mercury from the complex matrix prior to μPD-OES analysis, enabling sensitive and accurate determination of soil mercury. To our knowledge, the combination of EMHV and P&T for soil mercury analysis using microplasma atomic spectrometry has not been previously reported. Initial experiments were conducted to assess the feasibility and practicality of EMHV-P&T-μPD-OES for quantifying mercury in soil samples. A 50 mg soil CRM (GBW07980) was weighed and placed in a sample boat, which was then inserted into the electromagnetic heating vaporization device. A 30 V of AC input voltage was applied to the electromagnetic induction unit, and a 100 mL min^{-1} of Ar was used as the purge gas to sweep mercury vapor, volatile organic compounds, and water vapor through the P&T unit. Concurrently, the temperature of the sample boat increased rapidly. After heating for 1 minute, the input voltage was switched off, but the Ar purge gas continued to flow through the vaporization tube. After 5 minutes of purging, the flow direction of the purge gas was altered to pass directly through the gold-sand trap and into the PD discharge chamber. Upon stabilizing the microplasma signal, a 20 V input power was activated to heat the quartz adsorption tube, desorbing the analyte from the gold-sand

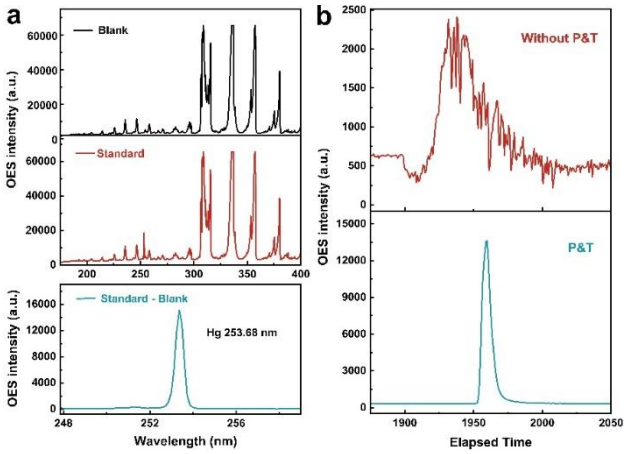

Fig. 3 (a) Typical optical emission lines for blank sample and standard samples generated with EMHV-P&T-μPD -OES using Ar as discharge gas, and mercury emission spectra after calibration with a 50 mg soil CRM (GBW07980). (b) Temporal emission profile of soil CRM obtained by EMHV-μPD-OES with and without P&T unit.

and sweeping it into the discharge chamber for detection. The signals collected by the charge-coupled device (CCD) are displayed in Fig. 3a. Besides the typical molecular emission spectral lines, such as OH (309 and 319 nm), N_2 (358 and 380 nm), and NH (337 nm), observed in both the blank and standard samples, the characteristic atomic emission line of mercury (253.7 nm) was clearly detected after subtracting the blank background. Additionally, 50 mg of soil CRM was determined by EMHV-μPD-OES in the presence or absence of the P&T unit and the results are displayed in Fig. 3b. These results confirm the advantage of the proposed method, wherein interference from the soil matrix is effectively eliminated before sample analysis.

Optimization of experimental parameters for EMHV. The EMHV parameters influencing Hg signal intensity, including sample consumption, evaporation voltage, and electromagnetic induction heating time were investigated.

Due to the limited capacity of the sample boat, the thickness of the soil layer increases when the amount of soil sample is too large. This may cause uneven heating of the sample and inefficient analyte release, thus reducing the accuracy of the detection results. Therefore, it was necessary to investigate the maximum soil carrying capacity of the sample boat. Standard soil samples ranging of 20-80 mg were tested, and the results are presented in Fig. 4a. When the soil amount reached exceeded 60 mg, the signal no longer increased. During the experiment, the issue might arise from the fact that when using 60 mg of soil, it only covered the bottom of the sample boat. As the sample amount increased, the thickness of the soil layer also increased, which hindered the release of soil mercury. Therefore, the amount of soil sample for subsequent experiments should be controlled within 60 mg.

The vaporization voltage of soil mercury directly affects the efficiency of mercury generation in the electromagnetic heating vaporization method. When the voltage is low, the temperature generated in the sample boat is also low. This hinders the process of mercury atomization and release, resulting in lower detection outcomes and lower instrument accuracy. Excessively high voltage can lead to increased energy consumption, which is not favourable for development of portable instruments. As depicted in Fig. 4b, the mercury signal intensity reaches a peak at 30 V, after which there is no significant change. Therefore, 30 V was used as the optimal voltage for mercury vaporization in subsequent experiments.

The duration of the heating time is a crucial factor in device design and its energy consumption. With the extension of heating time, the heat production generated by the electromagnetic induction device itself increases. When the device overheats, it becomes necessary to incorporate a water-cooling system to lower the temperature and ensure normal operation of the device. However, this unavoidably increases the size and energy consumption of the device, which is not favourable for the development of portable instruments. For this reason, we investigated the heating duration of soil samples, and the results are shown in Fig. 4c. After 20 seconds, the signal reaches a plateau and remains relatively stable thereafter. Therefore, in subsequent experiments, the heating time was limited to 20 seconds. Throughout this period, the temperature of the electromagnetic induction module itself did not change significantly. As a result, water-cooling could be avoided in the device's design, further reducing in the device's volume.

Optimization of experimental parameters for P&T. The P&T parameters influencing Hg signal intensity, including purge carrier gas flow rate, purge time, and desorption voltage were investigated.

The purge carrier gas (Ar) flow rate not only affects the analysis time but also determines the adsorption efficiency of mercury atoms in gold-sand. Therefore, this experiment explored the change in mercury signal intensity with varying purge carrier gas flow rates in the range of 50-250 mL min^{-1}. The results are presented in Fig. 4d. When the flow rate is 100 mL min^{-1}, the signal intensity of mercury reaches the maximum value. When the flow rate is low, the carrier gas can't effectively transport mercury atoms generated by electromagnetic heating vaporization to the gold-sand for enrichment. When the flow rate is high, the contact time between mercury atoms and gold-sand is short, which reduces the capture efficiency of the adsorbent. To achieve the best performance of this method, a flow rate of 100 mL min^{-1} was thus chosen as the optimal purge carrier gas flow rate in the experiments.

In addition to the purge carrier gas flow rate, the purging time is also a crucial factor that affecting the efficiency of adsorbent

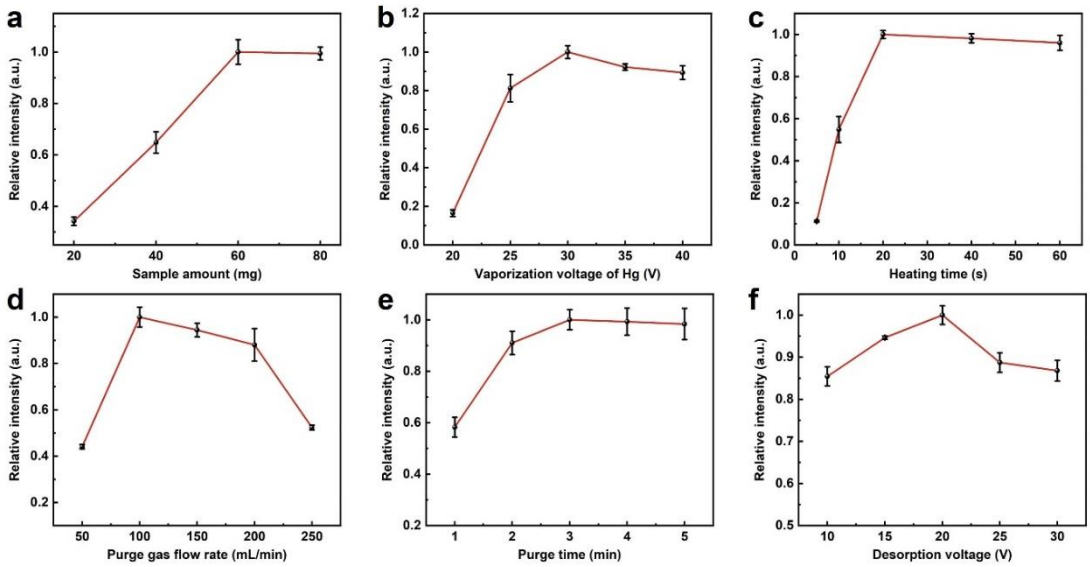

Fig. 4 Effect of (a) sample amount, (b) vaporization voltage of Hg, (c) heating time (d) purge gas flow rate, (e) purge time, and (f) desorption voltage on the responses from 240 μg/kg of Hg.

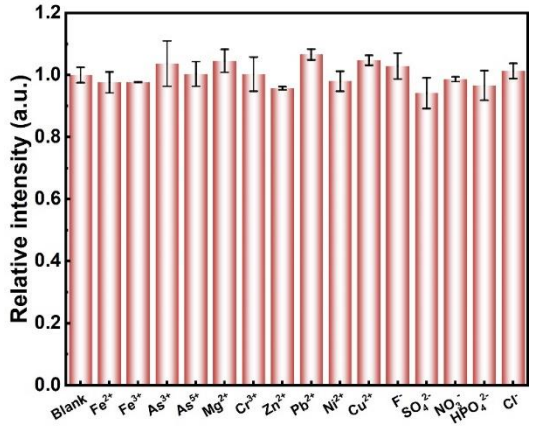

Fig. 5 The effect of different ions on the determination of Hg (Fe^{2+}, Fe^{3+}, As^{3+}, As^{5+}, Mg^{2+}, Cr^{3+}, Zn^{2+}, Pb^{2+}, Ni^{2+}, Cu^{2+}, F^-, SO_4^{2-}, NO_3^-, HPO_4^{2-}, and Cl^-) at a concentration of 240 μg/kg.

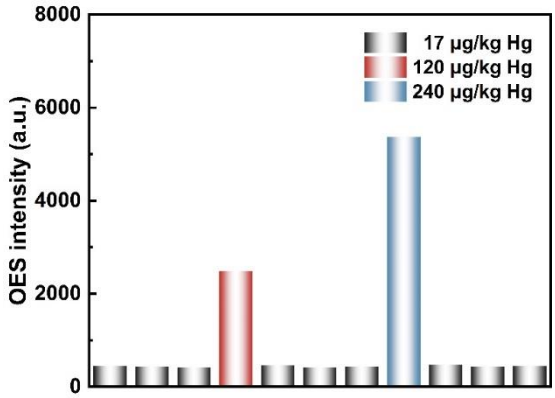

Fig. 6 Evaluation of the memory effect produced by EMHV-P&T-μPD-OES.

capture. Therefore, the relationship between the purge time and the mercury signal intensity was investigated at the optimal purge carrier gas flow rate. As shown in Fig. 4e, when the purge time exceeds 3 minutes, the intensity of the mercury signal reaches a plateau and remains constant with increasing time. Therefore, the purge time for all subsequent experiments was 3 min.

In this work, the thermal desorption was ach external heating by winding a nichrome wire (0.5 mm). The nichrome wire was tightly wrapped around the outer wall of the quartz tube. The temperature during thermal desorption was primarily controlled by the input voltage applied to both ends of the nichrome wire. Therefore, we investigated the variation of the mercury signal strength within the voltage range of 10-30 V. The results are depicted in the Fig. 4f. When the voltage is 20 V, the mercury signal intensity reaches the maximum value. Therefore, 20 V was chosen as the optimal analysis voltage in this experiment.

Optimization of experimental parameters for μPD-OES. The μPD-OES parameters influencing Hg signal intensity, including discharge gas flow rate, discharge voltage, and discharge gap were investigated. The results are summarized in Fig. S1. The following conditions were optimal for the proposed instrument: discharge gas flow rate, 80 mL min^{-1}; discharge voltage, 2.18 kV; and discharge gap, 3 mm.

Interferences. The environmental soil samples had complex compositions containing abundant inorganic elements. To explore the potential effects of inorganic ions on soil mercury detection, a series of 20 mg soil samples (GBW07980, Hg: 0.24 mg kg^{-1}) were supplemented with 0.5 μg of common cations and anions, including Fe^{2+}, Fe^{3+}, As^{3+}, As^{5+}, Mg^{2+}, Cl^-, Zn^{2+}, Pb^{2+}, Ni^{2+}, Cu^{2+},

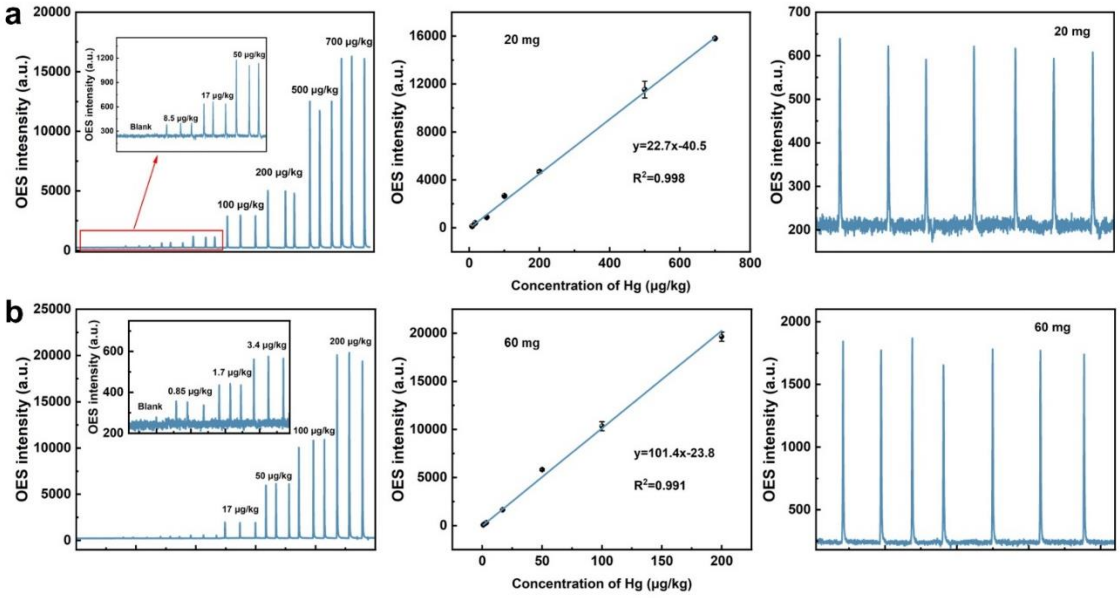

Fig. 7 Effect of (a) sample amount, (b) vaporization voltage of Hg, (c) heating time (d) purge gas flow rate, (e) purge time, and (f) desorption voltage on the responses from 240 μg/kg of Hg.

Table 1. Analytical results for determination of Hg in CRM soil

Samples	Certified value, (mg kg^{-1}) [a]	Found (mg kg^{-1}) [a]	T-value
GBW07403a	0.116 ± 0.005	0.115 ± 0.005	0.35
GBW07303a	0.067 ± 0.004	0.068 ± 0.002	0.87

[a]Mean and standard deviation results ($t_{0.05,2}$ = 4.30; P =95%; n= 3)).

F^-, SO_4^{2-}, NO_3^-, HPO_4^{2-}, and Cl^-. These samples were analyzed by EMHV-P&T-μPD-OES. As illustrated in Fig. 5, recoveries ranging from 91% to 107% for Hg were obtained, indicating no significant interference from the tested ions in the soil. It can be concluded that the proposed method demonstrates excellent anti-interference capabilities and high selectivity.

Memory effect. To assess the potential memory effect of EMHV-P&T-μPD-OES, particularly whether residues remain in soil samples containing high concentrations of mercury after analysis by this method, this experiment evaluated the impact on the intensity of mercury emission signals at three different concentrations (17 μg kg^{-1}, 120 μg kg^{-1}, and 240 μg kg^{-1}) of CRM soil. Initially, the CRM soil (17 μg kg^{-1}) underwent three tests. This was followed by a test of the CRM soil (120 μg kg^{-1}) and another measurement of the CRM soil (17 μg kg^{-1}). As shown in Fig. 6, there was no significant difference in the signal intensity of mercury emission in the CRM soil (17 μg kg^{-1}). The experiment was then repeated with the CRM soil (240 μg kg^{-1}), yielding consistent results. Therefore, no evident memory effects were observed using this experimental method.

Analytical performance. To assess the analytical performance of the EMHV-P&T-μPD-OES system, soil samples containing various concentrations of mercury were analyzed under optimal conditions with sample amounts of 20 and 60 mg. Since a soil CRM with a specific mercury concentration was unavailable, soil samples with adjusted concentrations were mixed with quartz sand and three CRM soils (GSS-2a, GSS-38, and GSS-7a) for analysis. The plot of the Hg atom emission signal intensity versus soil Hg concentration and the obtained standard curve are shown in Fig. 7. The linear correlation coefficient (R^2) for the two standard curves exceeded 0.99. The limits of detection (LODs), defined as the analyte concentration equivalent to three times the standard deviation of 11 repeated measurements of the blank solutions, were 1 μg kg^{-1} and 0.25 μg kg^{-1} for sample consumptions of 20 mg and 60 mg, respectively. The precisions, expressed as the relative standard deviations (RSDs) of 7 repeated measurements of CRM soil (GSS-2a) were greater than 3.8%. Table. S2 summarizes the analytical performance of this method compared with other similar methods, indicating that the EMHV-P&T-μPD-OES system demonstrates comparable or better sensitivity and stability. These results suggest that EMHV-P&T-μPD-OES offers significant potential for the field detection of trace mercury in soil samples.

Sample Analysis. Two CRM soils (GSS-3a and GSD-3a) were analyzed using EMHV-P&T-μPD-OES to verify the accuracy of the proposed method (Table 1). The *t*-test results indicate that the values obtained using this method are consistent with the CRM certification values (GSD-3a: 0.116 mg kg^{-1}; GSS-3a: 0.067 mg kg^{-1}). Five real soil samples collected from different regions (Chengdu, Chongqing, Chengdu, Dalian, and Neijiang) were

Table 2. Analytical results for determination of Hg in five real soil samples

Samples	This method (mg kg^{-1}) [a]	HG-AFS (mg kg^{-1}) [a]	T-value
1	0.032 ± 0.001	0.034 ± 0.001	2.44
2	0.049 ± 0.002	0.052 ± 0.001	2.15
3	1.412 ± 0.083	1.477 ± 0.028	1.28
4	0.072 ± 0.004	0.079 ± 0.002	2.71
5	0.240 ± 0.014	0.266 ± 0.040	2.06

analyzed (Table 2). The reliability of the experimental results was assessed using HG-AFS (GB/T 22105.1). According to the *t*-test results, there was no significant difference between the results of the two analyses within a 95% confidence interval. These findings demonstrate that the proposed method exhibits excellent analytical accuracy and feasibility.

CONCLUSION

A portable device integrating miniature purge-and-trap with EMHV-μPD-OES was designed and fabricated for the sensitive field detection of soil mercury without chemical pretreatment. The electromagnetic heating unit of EMHV-P&T-μPD-OES directly heats the soil sample and converts soil mercury species to mercury cold vapor. The generated Hg^0, along with the volatile sample matrix, is then swept from the soil sample and selectively captured and pre-concentrated by the purge-and-trap unit prior to μPD-OES analysis. The developed analytical system not only eliminates the tedious sample digestion but also separates mercury species from complex sample matrix, thus simplifying the analytical procedure and enhancing the sensitivity and anti-interference capability of microplasma OES for the field detection of soil mercury. Moreover, the proposed method also offers several advantages, such as low cost and simple operation and eliminates the use of toxic reagents, thus exhibiting great potential for the field detection of soil mercury.

ASSOCIATED CONTENT

The supporting information (Tables S1-S2 and Fig. S1) is available at www.at-spectrosc.com/as/home

AUTHOR INFORMATION

Chengbin Zheng is currently a professor of environmental analytical chemistry in the College of Chemistry of Sichuan University. He received his B.S. and Ph.D. degrees from Sichuan University and successively worked as a postdoctoral researcher at the National Research Council Canada and the Research Center for Eco-Environmental Science, Chinese Academy of Sciences. His current research focuses on the development of field analytical methods and instruments for environmental analysis. He has been working as editorial board of *Atomic Spectroscopy*.

Yurong Deng is currently a lecturer in the College of Chemistry of Sichuan University. She received her B.S. and M.S. degrees from Sichuan University and her Ph.D. degree from the University of New Mexico, USA. Her current research interests are focused on scientific issues in environmental analysis, developing new methods for field analysis, and addressing environmental pollution problems.

Corresponding Author

*C. B. Zheng

Email address: abinscu@scu.edu.cn

*Y. R. Deng

Email address: ydeng@scu.edu.cn

Notes

The authors declare no competing financial interest.

ACKNOWLEDGMENTS

The authors gratefully thank the National Nature Science Foundation of China (No. 22076128) for financial support of this work.

REFERENCES

1. R. Chen, A. de Sherbinin, C. Ye, and G. Shi, *Science*, 2014, **344**, 691-691. https://doi.org/10.1126/science.344.6185.691-a
2. D. Hou, D. O'Connor, A. D. Igalavithana, D. S. Alessi, J. Luo, D. C. W. Tsang, D. L. Sparks, Y. Yamauchi, J. Rinklebe, and Y. S. Ok, *Nat. Rev. Earth Environ.*, 2020, **1**, 366-381. https://doi.org/10.1038/s43017-020-0061-y
3. Y. Hu, S. Yang, H. Cheng, and S. Tao, *Environ. Sci. Technol.*, 2022, **56**, 17604-17614. https://doi.org/10.1021/acs.est.2c01854
4. Y. Liu, C. Wen, and X. Liu, *Science*, 2013, **339**, 1382-1383. https://doi.org/10.1126/science.339.6126.1382-b
5. H. Liu, J. Zhou, M. Li, R. Xia, X. Wang, and J. Zhou, *Environ. Sci. Technol.*, 2022, **56**, 12734-12744. https://doi.org/10.1021/acs.est.2c04062
6. Y. Mao, H. Tan, M. Wang, T. Jiang, H. Wei, W. Xu, Q. Jiang, H. Bao, Y. Ding, F. Wang, and C. Zhu, *J. Agric. Food. Chem.*, 2022, **70**, 8513-8522. https://doi.org/10.1021/acs.jafc.2c01437
7. M. Sánchez-Báscones, J. M. Antolín-Rodríguez, P. Martín-Ramos, A. González-González, C. T. Bravo-Sánchez, and J. Martín-Gil, *J. Soils Sediments*, 2016, **17**, 927-935. https://doi.org/10.1007/s11368-016-1622-z

8. N. Y. Ho, L. Yang, J. Legradi, O. Armant, M. Takamiya, S. Rastegar, and U. Strähle, *Environ. Sci. Technol.*, 2013, **47**, 3316-3325. https://doi.org/10.1021/es3050967
9. Y. Sun, Q. Zhou, and J. Zheng, *Environ. Int.*, 2019, **132**, 105115. https://doi.org/10.1016/j.envint.2019.105115
10. G. Aragay, J. Pons, and A. Merkoçi, *Chem. Rev.*, 2011, **111**, 3433-3458. https://doi.org/10.1021/cr100383r
11. Y. Wang, Y. Lin, T. Ren, Y. Yang, Z. He, Y. Deng, and C. Zheng, *Anal. Chem.*, 2023, **95**, 10873-10878. https://doi.org/10.1021/acs.analchem.3c00686
12. T. Liu, J. Liu, X. Mao, X. Huang, and Y. Qian, *Anal. Chem.*, 2023, **95**, 594-601. https://doi.org/10.1021/acs.analchem.2c04438
13. Z. Lv, J. Liu, X. Mao, X. Na, and Y. Qian, *Anal. Chim. Acta*, 2022, **1231**, 340444. https://doi.org/10.1016/j.aca.2022.340444
14. R. Yi, X. Yang, R. Zhou, J. Li, H. Yu, Z. Hao, L. Guo, X. Li, Y. Lu, and X. Zeng, *Anal. Chem.*, 2018, **90**, 7080-7085. https://doi.org/10.1021/acs.analchem.8b01756
15. J. Nie, L. Guo, Y. Liu, N. Deng, Z. Hu, P. Zheng, and C. Lau, *Talanta*, 2024, **267**, 125199. https://doi.org/10.1016/j.talanta.2023.125199
16. M. Qu, X. Guang, H. Liu, Y. Zhao, and B. Huang, *Environ. Pollut.*, 2022, **292**, 118324. https://doi.org/10.1016/j.envpol.2021.118324
17. M. Wan, W. Hu, M. Qu, K. Tian, H. Zhang, Y. Wang, and B. Huang, *Ecol. Indic.*, 2019, **101**, 583-594. https://doi.org/10.1016/j.ecolind.2019.01.069
18. Y. Jia, H. Yu, L. Wu, X. Hou, L. Yang, and C. Zheng, *Anal. Chem.*, 2015, **87**, 5866-5871. https://doi.org/10.1021/acs.analchem.5b00712
19. Y. Luo, Y. Yang, Y. Lin, Y. Tian, L. Wu, L. Yang, X. Hou, and C. Zheng, *Anal. Chem.*, 2018, **90**, 1547-1553. https://doi.org/10.1021/acs.analchem.7b04376
20. P. Chen, Y. Deng, K. Guo, X. Jiang, C. Zheng, and X. Hou, *Microchem. J.*, 2014, **112**, 7-12. https://doi.org/10.1016/j.microc.2013.09.009
21. Y. Su, X. Pan, Y. Lin, Y. Deng, and C. Zheng, *Atom. Spectrosc.*, 2023, **44**, 76-83. https://doi.org/10.46770/AS.2023.091
22. S. Liu, X. Xue, Y. Yu, and J. Wang, *Anal. Chem.*, 2021, **93**, 6262-6269. https://doi.org/10.1021/acs.analchem.1c00819
23. M. Zhang, Q. Tang, P. Li, L. He, X. Hou, and X. Jiang, *Anal. Chem.*, 2023, **95**, 5151-5158. https://doi.org/10.1021/acs.analchem.3c00306
24. J. Yang, Y. Lin, L. He, Y. Su, X. Hou, Y. Deng, and C. Zheng, *Anal. Chem.*, 2021, **93**, 14923-14928. http://doi.org/10.1021/acs.analchem.1c02023
25. J. Gu, S. R. Oliveira, G. L. Donati, J. A. Gomes Neto, and B. Jones, *Anal. Chem.*, 2011, **83**, 2526-2531. https://doi.org/10.1021/ac1027897
26. S. Xia, A. Leng, Y. Lin, L. Wu, Y. Tian, X. Hou, and C. Zheng, *Anal. Chem.*, 2019, **91**, 2701-2709. https://doi.org/10.1021/acs.analchem.8b04222
27. A. Kitano, A. Iiduka, T. Yamamoto, Y. Ukita, E. Tamiya, and Y. Takamura, *Anal. Chem.*, 2011, **83**, 9424-9430. https://doi.org/10.1021/ac2020646
28. A. Leng, Y. Lin, Y. Tian, L. Wu, X. Jiang, X. Hou, and C. Zheng, *Anal. Chem.*, 2017, **89**, 703-710. https://doi.org/10.1021/acs.analchem.6b03185
29. X. Liu, Z. Liu, Z. Zhu, D. He, S. Yao, H. Zheng, and S. Hu, *Anal. Chem.*, 2017, **89**, 3739-3746. https://doi.org/10.1021/acs.analchem.7b00126
30. C. Zheng, L. Hu, X. Hou, B. He, and G. Jiang, *Anal. Chem.*, 2018, **90**, 3683-3691. https://doi.org/10.1021/acs.analchem.7b04759
31. J. Yang, Y. Luo, Y. Su, Y. Li, Y. Lin, and C. Zheng, *Microchem. J.*, 2022, **179**, 107569. https://doi.org/10.1016/j.microc.2022.107569
32. L. He, Y. Lin, P. Chen, Y. Su, Y. Li, and C. Zheng, *J. Hazard. Mater.*, 2022, **439**, 129607. https://doi.org/10.1016/j.jhazmat.2022.129607
33. B. Han, X. Jiang, X. Hou, and C. Zheng, *Anal. Chem.*, 2014, **86**, 936-942. https://doi.org/10.1021/ac403662w
34. Z. Zhu, G. C. Y. Chan, S. J. Ray, X. Zhang, and G. M. Hieftje, *Anal. Chem.*, 2008, **80**, 8622-8627. https://doi.org/10.1021/ac801531j
35. A. Leng, Y. Tian, M. Wang, L. Wu, K. Xu, X. Hou, and C. Zheng, *Chin. Chem. Lett.*, 2017, **28**, 189-196. https://doi.org/10.1016/j.cclet.2016.06.056
36. C. Yang, G. Chan, D. He, Z. Liu, Q. Deng, H. Zheng, S. Hu, and Z. Zhu, *Anal. Chem.*, 2019, **91**, 1912-1919. https://doi.org/10.1021/acs.analchem.8b03944
37. C. Yang, D. He, Z. Zhu, H. Peng, Z. Liu, G. Wen, J. Bai, H. Zheng, S. Hu, and Y. Wang, *Anal. Chem.*, 2017, **89**, 3694-3701. https://doi.org/10.1021/acs.analchem.6b05158
38. X. Peng and Z. Wang, *Anal. Chem.*, 2019, **91**, 10073-10080. https://doi.org/10.1021/acs.analchem.9b02006
39. J. Mo, Q. Li, X. Guo, G. Zhang, and Z. Wang, *Anal. Chem.*, 2017, **89**, 10353-10360. https://doi.org/10.1021/acs.analchem.7b02214
40. C. Yang, G. Cheng, S. Cheng, X. Liu, Y. Liu, H. Zheng, S. Hu, and Z. Zhu, *Anal. Chem.*, 2021, **93**, 16393-16400. https://doi.org/10.1021/acs.analchem.1c02940
41. J. Cai, X. Zhang, Y. Wei, S. Chen, Y. Yu, and J. Wang, *Anal. Chem.*, 2024, **96**, 3733-3738. https://doi.org/10.1021/acs.analchem.3c05330
42. F. Ge, L. Gao, X. Peng, Q. Li, Y. Zhu, J. Yu, and Z. Wang, *Talanta*, 2020, **218**, 121119. https://doi.org/10.1016/j.talanta.2020.121119
43. Y. Deng, J. Hu, M. Li, L. He, K. Li, X. Hou, and X. Jiang, *Anal. Chim. Acta*, 2021, **1163**, 338502. https://doi.org/10.1016/j.aca.2021.338502
44. H. Jiang, Y. Qin, and B. Hu, *Talanta*, 2008, **74**, 1160-1165. https://doi.org/10.1016/j.talanta.2007.08.022
45. P. Li, J. Hu, M. Zhang, L. He, K. Li, X. Hou, and X. Jiang, *Anal. Chem.*, 2022, **94**, 7683-7691. https://doi.org/10.1021/acs.analchem.2c01105
46. X. Jiang, Y. Chen, C. Zheng, and X. Hou, *Anal. Chem.*, 2014, **86**, 5220-5224. https://doi.org/10.1021/ac500637p
47. H. R. Badiei, B. Lai, and V. Karanassios, *Spectroc. Acta B,* 2012, **77**, 19-30. https://doi.org/10.1016/j.sab.2012.07.025
48. Z. Cai, L. Qian, X. Peng, and Z. Wang, *Anal. Chem.*, 2021, **93**, 14701-14707. http://doi.org/10.1021/acs.analchem.1c03057
49. X. Liu, K. Yu, H. Zhang, X. Zhang, H. Zhang, J. Zhang, J. Gao, N. Li, and J. Jiang, *Talanta*, 2020, **219**, 121348. https://doi.org/10.1016/j.talanta.2020.121348
50. Z. He, Y. Lin, Y. Wang, L. He, X. Hou, and C. Zheng, *Anal. Chem.*, 2020, **92**, 9583-9590. https://doi.org/10.1021/acs.analchem.0c00755
51. Y. Su, Y. Lin, Y. Li, T. Ren, Y. Deng, and C. Zheng, *Anal. Chim. Acta*, 2023, **1261**, 341184. https://doi.org/10.1016/j.aca.2023.341184
52. S. Zhang, H. Luo, M. Peng, Y. Tian, X. Hou, X. Jiang, and C. Zheng, *Anal. Chem.*, 2015, **87**, 10712-10718. https://doi.org/10.1021/acs.analchem.5b02820